Rafael de Lima Lemos
Graduate Student
School of Engineering
Universidade Federal do Rio Grande
Brazil

Rodrigo Spotorno Vieira
Assistant Professor
School of Engineering
Universidade Federal do Rio Grande
Brazil

Liércio André Isoldi
Adjunct Professor
School of Engineering
Universidade Federal do Rio Grande
Brazil

Luiz Alberto Oliveira Rocha
Adjunct Professor
Department of Mechanical Engineering
Universidade Federal do Rio Grande do Sul
Brazil

Martim dos Santos Pereira
Graduate Student
School of Engineering
Universidade Federal do Rio Grande
Brazil

Elizaldo Domingues dos Santos
Adjunct Professor
School of Engineering
Universidade Federal do Rio Grande
Brazil

Numerical Analysis of a Turbulent Flow with Coanda Effect in Hydrodynamics Profiles

In the naval industry, hydrofoils are used for generating lift in low-friction vessels, minimizing drag forces between the surrounding fluid and the hull. These devices are also applied to keep stability and maneuverability for high-speed vessels. A recent technology based on Coanda effect for flows over hydrodynamic profiles has been developed for the application of this equipment to increase the flow, converting lifting forces into propelling ones, aiming to attend the industry interest for developing improved nautical propulsion mechanisms. The main purpose of the present work is to simulate the main operational principle of a hydro-propulsion device based on the Coanda effect. More precisely, a turbulent water flow in two hydrodynamic profiles is considered. The mass flow rate of water in the device is thoroughly studied in this work, solving numerically time-averaged conservation equations of mass and momentum with Computational Fluid Dynamics (CFD) code based on the Finite Volume Method (FVM). To tackle with closure modeling for turbulence it is employed the standard k - ε model. The effect of distance between two hydrodynamic profiles over the mass flow rate is also studied. Results obtained here show that the multiplying effect is noticed in water flow in the region between two hydrodynamic profiles, which is similar to previous findings of the literature for the air flow through aerodynamic profiles submitted to Coanda effect.

***Keywords**: Coanda effect, Hydropropulsion, Flow Amplification, CFD*

1. INTRODUCTION

Flow amplification devices work through a known physical concept. The first device based on this effect was patented by the Romanian inventor and aeronautical engineer Henri Coanda in 1936 [1].

The Coanda effect in a simple description is the tendency of a fluid flow to adhere to a curved surface due to local pressure reduction by the acceleration of a fluid around a surface [2,3]. As a natural phenomenon, Coanda effect describes the tendency of a fluid jet to be attracted to a nearby surface (flaps or airfoils). This adherence can be controlled either by injecting a fine jet of tangential fluid to the curved surface or by operating a control jet, forcing the main jet to attach itself to the wall. Some studies explaining the physical principle can be seen in the literature [2-6]. To reach that purpose, the so called Coanda surfaces are profiles that are characterized by a significant asymmetry, and in that perspective, it can be possible to modify the properties of a flow that runoff on any surface that have those characteristics [7-11].

In the naval industry, it is relatively common to find the use of hydrofoils in low friction vessels. Usually, they have the function of generating a lift effect on boat hulls, or reducing the friction between the hull and the water [12,13]. Also, the study of aerodynamics and hydrodynamics effects is vital for the development of any moving vehicle, be it marine, terrestrial or aeronautical. It provides the foundation needed for the development of more efficient machines at a lower energy costs, that is, with less drag it is possible to move more with the same amount of energy. An example of this application can be found in similar studies like the references [14,15]. Also, by encouraging the study and applications of eco-friendly technologies, wasting less energy and increasing the efficiency of marine vehicles, we take a step closer towards the concept of "green logistics" [16].

However, the practical application of the hydrofoils effects is difficult to obtain for large marine vessels, since each vessel needs a specific hydrofoil that supports the exact load that can be carried. For this reason, these types of hydrofoils are generally more commonly used in sports boats, used in racing boats.

In recent studies, the utilization of the Coanda Effect through hydrofoils to improve the efficiency and amplify flow in new devices has been theoretically studied with the employment of CFD software [2-11]. The simulation of fluid flow over hydrofoils has been done with the purpose to create propulsion devices using the flow amplification effect.

In the literature, most of applications used fluid-film jets tangentially impinged on surfaces to generate lift

Received: January 2017, Accepted: February 2017
Correspondence to: Rafael de Lima Lemos
Universidade Federal do Rio Grande
Avenida Itália, km 8, CP. 474, Rio Grande, RS, Brazil
E-mail: er.lemos@outlook.com
doi:10.5937/fmet1703412L

directly or indirectly [11]. With the correct arrangement, this effect could be optimized to the point of generating a significant increase in fluid flow through an induction process. The model presented in this paper was based on the study of a domestic ventilator performed by [9,10]. In these studies, acoustic efficiency as well as the amplification of mass flow rate in a small fan using air as working fluid are realized. Much of the studies related to this phenomenon are devoted to flows with low density (e.g., air) due to the lower energy demand to obtain the amplifying effect. If the same effect can be reproduced in flow machines that move fluids with high density, such as water, it would be possible to reduce costs in the acquisition of equipment, operation and maintenance, since the energy consumption to generate the desired flow can be significantly reduced.

In the present work, a theoretical device is numerically simulated by an analysis of water jet, impelled tangentially to a curved surface (Coanda surface), to generate a turbulent flow by nozzles fixed in the hydrodynamic profiles themselves. The Coanda effect is used to amplify the flow magnitude in the region between the hydrofoils. The main purpose here is to simulate the main operational principle of this kind of device for a flow with high density fluid. To the best of the author's knowledge, the evaluation of this kind of problem was not performed for a high-density fluid as water. Posteriorly, the effect of distance between the two adjacent hydrofoils over the mass flow rate in the region between the hydrofoils is performed, given a theoretical recommendation about the influence of this parameter over the device performance. For the simulation of incompressible, two-dimensional and turbulent flow the time-averaged conservation equations of mass and momentum are solved with the Finite Volume Method (FVM). The standard $k - \varepsilon$ model is used for closure of time-averaged equations.

2. THE PROBLEM DESCRIPTION

The computational domain and mesh generation are performed with the use of the software GAMBIT. Dimensions and geometries are similar to those of the models presented by [10]. However, the purpose in this paper is essentially the creation of a new model that uses other work fluid (water). Based on this premise, the domain presented here was recreated, using the guidelines of the models presented in the studies presented in the references.

To obtain more knowledge about how the geometry of the introduced new model may influence the results, fixed parameters of computational domain size and dimensions of the hydrofoil geometry are established. Figure 1 illustrates the computational domain and a detailed view of the hydrodynamic profiles, which are used to carry out the simulations presented in this work.

The main parameter of study was the distance between the profiles (d), Fig. 1(b). These are adjusted at twelve different magnitudes, where the x positions of profiles remained unchanged in all models, while the y position is changed to vary the distance from the two profiles (d). For the hydrofoils profiles, a standard length of the profile chord l is established (l = 1 m). The water was chosen as the high density working fluid for all simulations. Moreover, it is considered an incompressibility flow in two-dimensional domain incident on the solid surfaces. The domain has dimensions of L = 29.7 m and H = 25.5 m [Figure 1(a)]. In the hydrofoils, the nozzles where the fluid jet is ejected, have a standard height of b = 35 mm. The nozzles also form an angle parallel with z axis of the computational domain. The other surfaces of the hydrodynamic profiles have non-slip and impermeability boundary conditions [Figure 1(b)]. Since the thermal effects are neglected for solution of this case, the thermophysical properties are assumed at a temperature of 10º C, i.e., ρ = 998.2 kg/m³ and υ = 1.2671×10^{-6} m²/s. In the external lines of computational domain, Figure 1(a), it is imposed a prescribed atmospheric pressure (p_g = 0 atm).

It is worthy to mention that the sole mechanism for driving the fluid is the imposition of the velocity in the nozzles. For all simulations performed here it is imposed in the two nozzles a velocity V = 50 m/s which leads to a Reynolds number of $Re_l = 23{,}6 \times 10^6$ (where a characteristic length is the profile chord).

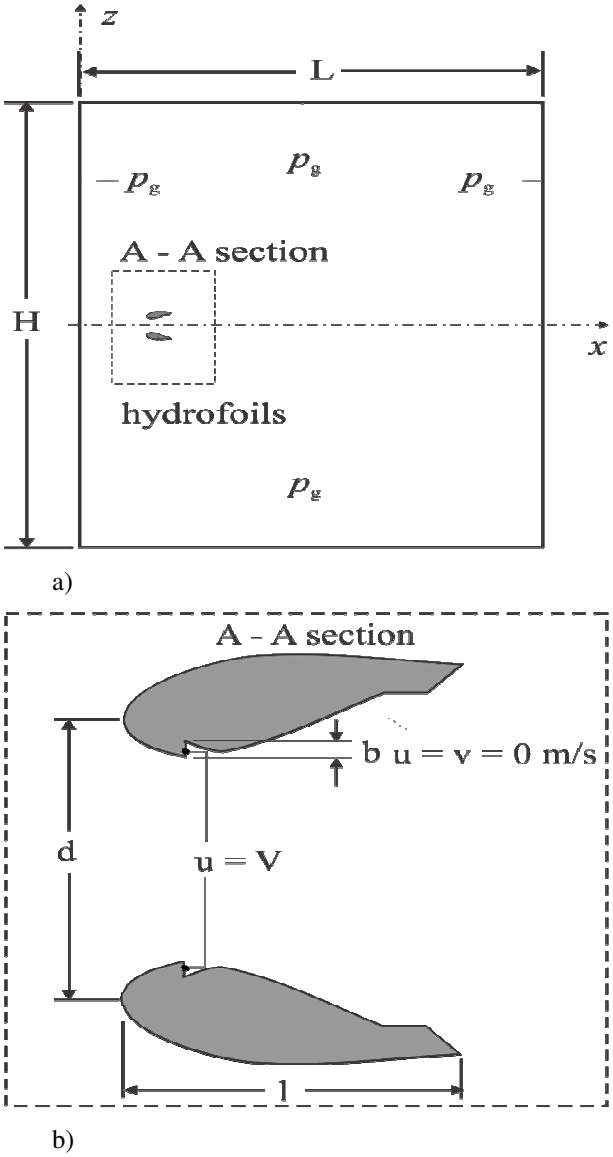

Figure 1. Dimensions of the computational domain: a) general view, b) detailed view in the device region.

In order to evaluate the amplification flux effect, the model also has two virtual lines (one in the entrance and other in the exit of the theoretical device), drawn in FLUENT with the intention of forming a control volume in the region between the two profiles. Thus, establishing these control lines, it is possible to analyse the flow rate in the inlet and outlet regions of the domain, such as the magnitudes of dynamic pressure and velocity magnitude. These monitoring lines are illustrated in the Figure 2. Figure 2 also shows a schematic sketch of how the problem was assembled, and how the fluid flow should behave in the simulations. The red arrows coming out of the nozzle region, eject the flow of fluid impinged on the surfaces, causing a negative pressure in the region between the hydrodynamic profiles and sucking fluid from upstream region of device. The blue arrow entering the control volume represents the fluid being sucked into the control region. Finally, in the exit region, there is a mixture between the two flows (the imposed at the nozzle and the sucked one between the profiles) which are represented here as blue and red arrows, respectively.

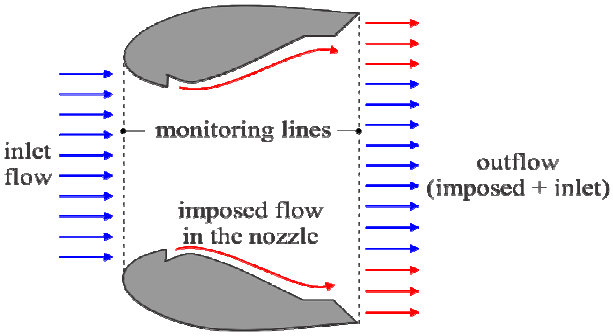

Figure 2. Behaviour expected by the fluid in the simulations processes.

In total, twelve different cases are simulated, so that, the effects that these distances generate in the flow on the pressure and velocity profiles, as well as, in the effect of amplification, are analysed. As mentioned previously, the parameter established in this work to refer to the distance between the profiles will be the entrance distance d of the control volume (see Figure 1). Table 1 shows the distances between the two profiles, measured in the entrance (d) and the exit (d_e) regions of the device, representing all studied cases of the present work.

Table 1. Distances tested in the simulations for this paper.

d (m)	d_e (m)
0.33	0.60
0.69	0.96
1.04	1.31
1.40	1.67
2.11	2.38
2.83	3.10
3.54	3.81
4.26	4.53
4.97	5.24
6.40	6.67
7.83	8.10
9.97	10.24

3. MATHEMATICAL AND NUMERICAL MODELING

The time-averaged conservation equations of mass and momentum are used to account for a turbulent and incompressible flow in a two-dimensional domain. These equations are suitable presented in literature [17,18,19]. The continuity equation is given by (1).

$$\frac{\partial \overline{u_i}}{\partial x_i} = 0 \tag{1}$$

Where u_i is the velocity in i-direction (i = 1 and 2, which represents as directions x and y, respectively). The time-averaged conservation of the momentum is described by (2).

$$\frac{\partial}{\partial t}(\rho \overline{u_i}) + \frac{\partial}{\partial x_i}(\rho \overline{u_{i\,i}}\overline{u_j}) = -\frac{\partial p}{\partial x_j} + \frac{\partial}{\partial x_j}\cdot$$

$$\left[\mu\left(\frac{\partial \overline{u_j}}{\partial x_i} + \frac{\partial \overline{u_j}}{\partial x_i} - \frac{2}{3}\delta_{ij}\frac{\partial \overline{u_k}}{\partial x_k}\right)\right] + \frac{\partial}{\partial x_j}\left(-\overline{\rho u_i' u_j'}\right) \tag{2}$$

where ρ is the fluid density, the Reynolds stresses (the term that needs to be modelled) are represented by the last term on the right side of the equality, and p denotes the pressure. The standard turbulence model k - ε is used by CFD software FLUENT to close the time-averaged equation, since additional terms arise from the average process. This method is used to simulate a turbulent flow through a semi-empirical mathematical model proposed by the reference [18]. Thus, the equations of k and ε are given by (3,4).

$$\frac{\partial}{\partial t}(\rho k) + \frac{\partial}{\partial x_i}(\rho u_i k) =$$

$$\frac{\partial}{\partial x_i}\left[\frac{\partial k}{\partial x_i}(\mu + \frac{\mu_t}{\sigma_k})\right] + G_k - \rho\varepsilon - Y_M + S_K \tag{3}$$

and:

$$\frac{\partial}{\partial t}(\rho \varepsilon) + \frac{\partial}{\partial x_i}(\rho u_i \varepsilon) =$$

$$\frac{\partial}{\partial x_i}\left[\frac{\partial \varepsilon}{\partial x_i}(\mu + \frac{\mu_t}{\sigma_\varepsilon})\right] + C_{\varepsilon 1}\frac{\varepsilon}{k}G_k - C_2\rho\frac{\varepsilon^2}{k} + S \tag{4}$$

In (3) and (4), G_k represents the turbulent kinetic energy rate, and Y_M represents the contribution of the floating expansion of the incompressible turbulence to the total dissipation rate. S_K and S_ε are parameters to be defined for each case. In this case, they were default values. The Reynolds stresses can be related to the rate of deformation of the mean field through the following expression showed in (5).

$$\overline{u_i' u_j'} = \frac{\mu_T}{\rho}\left(\frac{\partial \overline{v_i}}{\partial x_j} + \frac{\partial \overline{v_j}}{\partial x_i}\right) - \frac{2}{3}k\delta_{ij} \tag{5}$$

For this deduction, the viscosity takes the form described as showed in (6).

$$\mu_t = \rho C_\mu \frac{k^2}{\varepsilon} \tag{6}$$

Further details can be found in the work presented in the reference [18,20]. The values used in the variables are shown in Table 2.

Table 2. $k - \varepsilon$ constants employed in the numerical model.

$C\mu$	$C_{\varepsilon 1}$	$C_{\varepsilon 2}$	S_k	S_ε
0.09	1.44	1.92	1.0	1.3

The conservation equations of mass and momentum, as well as the differential equations of the turbulence model k - ε, are solved using the finite volume method (MVF) using FLUENT software [21].

Concerning the numerical modelling of the present simulations, the mesh generated in the computational domain for the elaboration of the simulations, was created in a two-dimensional plane, completely made of triangular cells (nearly 130,000 for all simulated cases). The triangular mesh was intensely refined in the regions of interest, such as the nozzles, the bulged surface (Coanda surface) and the boundary layer detachment region of the fluid. The solver selected to solve numerically the problem is pressure based. Moreover, once the flow is considered turbulent, the solution is performed in transient regime until the flow reaches the steady state. For velocity-coupling it is employed the algorithm SIMPLE and *second order upwind* for the treatment of advective terms in momentum and transport equations. In relation to residues, values of 10^{-6} were used for the equation of mass conservation, amount of movement and transport equations. All the solutions were simulated considering the transient regime. The time step used was 0.1 seconds, with 20 iterations per step and 1500 numbers of steps, totalling 30000 iterations and a physical simulation time of 150 s.

For the numerical simulation, a desktop computer with Intel i7 6950X CPU of 3.5 GHz and 16 Gb of RAM was used. The actual physical time elapsed for each of the simulated cases was around of four (4) to five (5) hours.

4. PROBLEM VERIFICATION

Once there is no reference in the literature about the water flow in a geometry similar to that proposed in the present work, verification is performed by comparison between the present model and turbulent flows of air over aerodynamic profiles. This model was designed to simulate and compare a numerical case of a simpler design, and results already published in the literature. The model chosen was a NACA4412 airfoil, widely used in the aircraft modelling industry, being, therefore, a case where the numerical approach has been successful in determining the drag, lift and pressure coefficients. Recommendation of the airfoil study was followed as provided in the *Cornell University* website tutorial [22]. An image of the model prepared per the *Cornell University* tutorial is presented in Figure 3.

Once several cases are simulated and the domain is highly complex, in the present work it is employed a triangular mesh with a strong refinement near the surfaces. Then, for the verification case this grid is tested and the results are compared with those presented in the literature. If the results for a turbulent flow over an airfoil is suitable, it can be assumed that the recommendations reached in the present work are also adequate. Figure 4 shows the mesh domain generated for this second model described here.

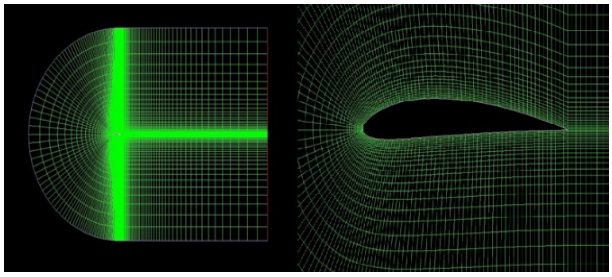

Figure 3. Computational domain of the model 1, per Cornell University.

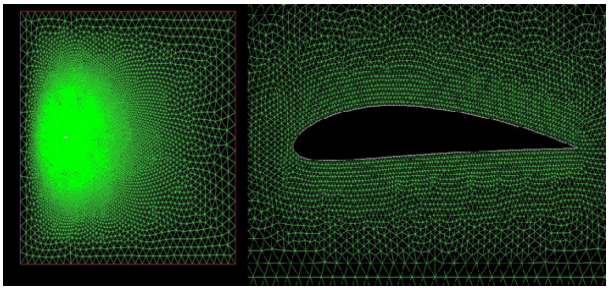

Figure 4. Computational domain of the model 2, created by the author.

Table 3 shows the comparison of the drag and lift coefficients obtained between the simulated models, and those presented in laboratory tests reported in the literature for the NACA4412 profile. The study presented in the reference [23], are in fact, values obtained through experimental analyses, under different flow conditions and different aerodynamic profiles. For the values presented in the table, the authors considered a null angle of attack and a Reynolds number of 3.0×10^6. Thus, it can be observed that the results presented in Table 3, show that the numerical model used here led to results in reasonable agreement with those presented in literature. It is worthy to mention that some differences can be found due to few magnitude of the values of lift and drag coefficient. The differences found are in agreement with those found in literature for this kind of simulation. Thus, the numerical model adopted here, can be extrapolated for the proposed device of flow amplification with water.

Table 3. Results of the verification process.

Reference	C_l	C_d
Cornell Model	0.6093	0.00567
Author Model	0.5813	0.00657
Abbott and Von Doenhoff [23]	0.5330	0.00700

5. RESULTS

Firstly, the velocity field between the hydrodynamic profiles is evaluated, as well as, the influence of the distance (d) over the velocity profiles in the inlet and outlet of theoretical device. Figure 5 shows the velocity profiles in the outlet region of the device. Firstly, two main peaks are observed for all simulated cases, i.e., independent of the distance between the hydrodynamic

profiles. These peaks happened due to the fluid impelled by the nozzles. It is also noticed that in the central region between the hydrodynamic profiles, the velocity magnitude is strongly smoothed, mainly for the highest distances d, where the velocity profile is almost constant. As the distance *d* decreases the velocity field in the intermediate region between the hydrodynamic profiles also increases, indicating the intensification of fluid flow in the region between the profiles caused by suction of fluid from the device upstream region.

Figure 6 shows the fluid velocity profiles at the inlet of the device. Results corroborate the findings noticed in Figure 5, i.e., the profiles configuration generates a fluid flow in the region between the hydrodynamic profiles. Moreover, for the lower magnitudes of *d*, the velocity in the intermediate region is intensified, showing the suction of fluid from the upstream region of device.

The velocity profiles in inlet region (Figure 5) have a kind of parabolic behaviour, which indicates a gain of velocity in the regions closer to the profiles. This gain is a product of the pressure gradient that causes an abrupt drop in pressure inside the devices and sucks the mass of fluid from the neighbouring regions. This phenomenon becomes more evident when one observes the profiles of total pressures, which will be introduced next.

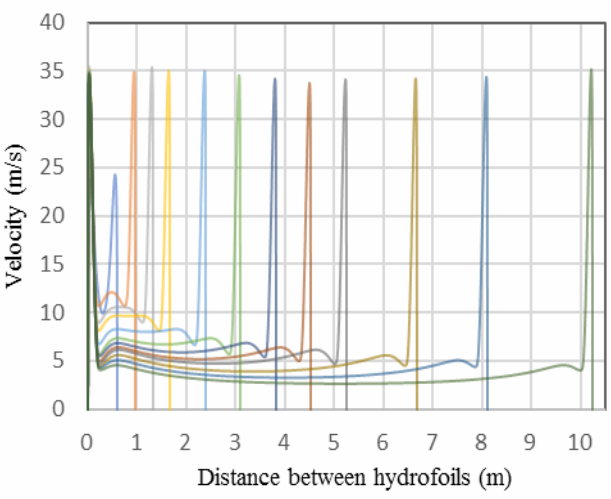

Figure 5. Velocity profiles in the outlet region of the devices.

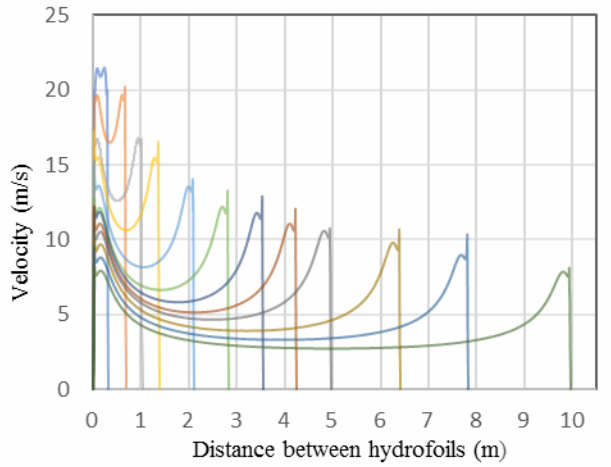

Figure 6. Velocity profiles in the inlet regions of the devices.

Another important parameter in the evaluation of the results are the total pressures resulting from the inlet and regions of the monitoring lines. The Figure 7 shows the values of the total pressure in the outlet region of device, where again as a function of the fluid ejected at high speed by the nozzles, the graphs indicate high magnitudes of total pressure at the extremes of the profiles, i.e., near the hydrodynamic profiles. Magnitudes near to 590 kPa are observed.

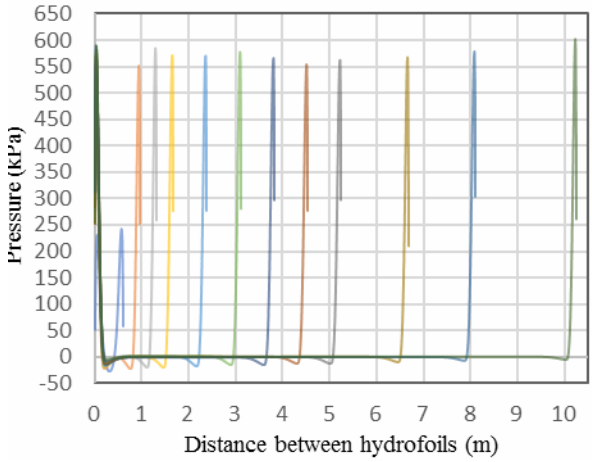

Figure 7. Total pressure profiles in the outlet region of the devices.

These regions of high pressure are responsible for the acceleration of the fluid at these points. This observation is compatible with the previously noticed for the velocity profiles. It can be also noticed a similar behaviour to that obtained for velocity profiles, where the total pressures caused by the nozzle jets have constant values in all cases. In the central zones of the graph, the pressures are much lower when compared to the pressures of the nozzle regions, being almost imperceptible in Figure 7. Even so, these zones have positive pressure values and are close to atmospheric pressure.

Figure 8 shows the total pressure profiles at the entrance of the devices, where pressure values are very close to 0 Pa (gauge). This observation is consistent with the observations of velocity profiles, since the input region of the equipment is sucking a mass of fluid in the vicinity of the control volume, which would only be possible with the hypothesis of a negative pressure gradient in this region. The inlet pressures have similar behaviour, however in this case there is a progressive decrease between the profiles as the hydrofoils profiles are removed. This observation indicates that the distance between the profiles actually interferes with the total pressures at the inlet, decreasing the intensity of the mean pressure gradient on the input monitoring line.

Also, to demonstrate in a clear and visual pattern the intensities of the pressure and velocity fields as the distances between the profiles increase, it is possible to visualize the contours of the pressure and velocity around the domains. Figure 9 shows an example of these contours, where only the distances cases of d = 2.1m, 2.8m, 3.5m and 4.2m are represented. It is possible to noticed that, with the distance, the magnitudes of the fields of velocity and pressure become smaller (represented by colder colours), both for speeds and for

pressures. This observation is adequate, since the results expressed (Figures 5 - 8), indicate the same tendency towards a decrease in pressure and velocity averages.

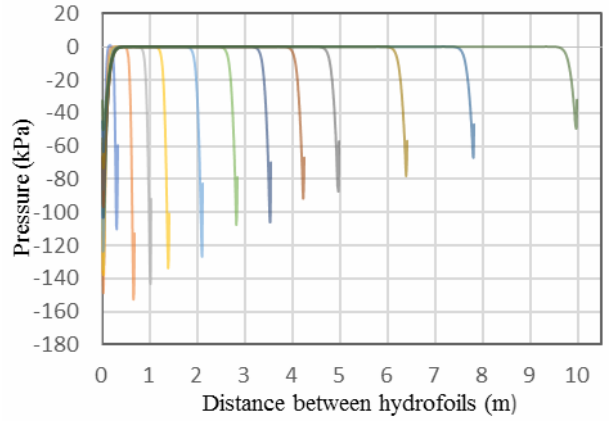

Figure 8. Total pressure profiles in the inlet region of the devices.

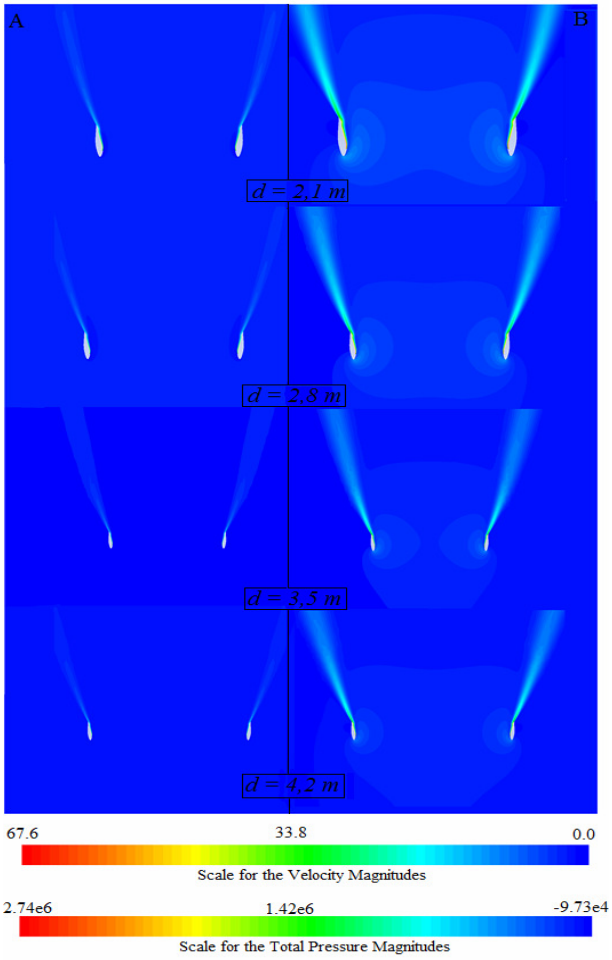

Figure 9. A) Total pressure contours; B) Velocity contours.

The figures also illustrate that the distance does not affect the intensity of the jets ejected by the nozzles, since it is maintained the same colour pattern in all cases. However, it can be seen that the jets tend to concentrate when the profiles are closer to each other, and with the distance, they become more dispersed. The pressure and velocity scales found alongside the pressure and velocity contours present identical maximum and minimum values in all cases. It should be noted that some small variations occur between simulations from one case to another. These scales, however, were fixed with these values in order to facilitate the visualization of magnitudes scale.

After determination of velocity profiles, it is possible to estimate the mean magnitude of velocity profiles (for each simulated distance d and the mass flow rate that crosses the inlet and outlet monitoring lines. The mean velocities obtained in the inlet and outlet can be seen in Table 4. As expected, results showed that the magnitude of mean velocity decreases with the increase of distance d.

Table 4. Average velocities in the inlet and outlet regions for each distance simulated.

d (m)	*Mean inlet velocity* (m/s)	*Mean outlet velocity* (m/s)
0.3	19.45	15.97
0.6	17.05	15.73
1.0	14.03	13.42
1.4	12.34	12.10
2.1	10.15	10.27
2.8	8.67	9.12
3.5	8.01	8.30
4.2	7.30	7.68
4.9	6.81	7.35
6.4	6.06	6.52
7.8	5.40	6.09
9.9	4.63	5.45

In possession of these values the mass flow rates for each distance (d) can be obtained by:

$$\dot{m}_n = V_n \cdot \rho_{water} \cdot A'_n \tag{7}$$

where $\dot{m}_n$ [kg/s.m], represents the mass flow rate for each distance d per unit depth since the problem is two-dimensional. V_n [m/s] represents the mean flow velocity for each distancing d. The variable ρ_{water} [kg/m³], is the water density, which is the same for all cases, and finally, A'_n [m²/m] represents the area which the fluid crosses, i.e., the product between the distance and the depth. With the use of (7) and the respective values in Table 4, it was possible to calculate the values shown in Table 5, where $\dot{m}_e$ indicates the mass flow rate at the inlet and $\dot{m}_s$ the mass flow rate at the outlet at each distancing between profiles, when imposed the condition in the nozzles of 50 m/s. Note that the values of mass flow rates in the nozzles do not vary in any of the cases.

Thus, the most enlightening way to elucidate the mass flow gain that this device could have, is through the ratio of mass flow rates between the outlets and those imposed on the nozzles. Following this premise, Table 6 presents the ratio of mass flow amplification (ε_m) as function of the distance between the profiles under the Coanda effect.

The mass flow behaviour is given as shown in Figure 10, where the superior line corresponds to mass flow rate at the outlet of device, and the inferior line corresponds to the mass flow rate at the inlet of device. The behaviour described in the figure illustrates coherently the previous findings reached in Table 6. The mass flow rates progressively increase in a very smooth

curve, indicating the existence of a probable point of maximum amplification ratio. The flow rates in the nozzles are identical in all cases simulated in this work, which also indicates that the increase in flow is due only to the increase in effective flow area.

Table 5. Average mass flow for each simulated distance.

d	$\dot{m}_e$	$\dot{m}_s$	$\dot{m}_b$
0.3	6471.4	9680.6	3563.5
0.6	11750.6	15141.1	3563.5
1.0	14667.6	17699.3	3563.5
1.4	17300.2	20274.2	3563.5
2.1	21461.6	24535.9	3563.5
2.8	24517.3	28301.5	3563.5
3.5	28354.8	31679.5	3563.5
4.2	31081.6	34794.3	3563.5
4.9	33857.1	38548.8	3563.5
6.4	38765.9	43474.0	3563.5
7.8	42273.1	49315.6	3563.5
9.9	46101.0	55801.0	3563.5

It is possible to note that the growth of the mass flow rate at the inlet and the mass flow rate in the outlet (the sum between the mass flow rates in the inlet and in the nozzle) are similar, with exception for $d > 7$ m, where the difference between the magnitudes increases. This fact indicates that the numerical model needs to be improved for large distances since the mass is not being conserved in the device. In spite of this fact, it is possible to observe a tendency of stagnation in the augmentation of amplification for high distances between the hydrodynamic profiles. Results (Figure 10) and Table 6, also shows that the device works very well in the amplification of flow.

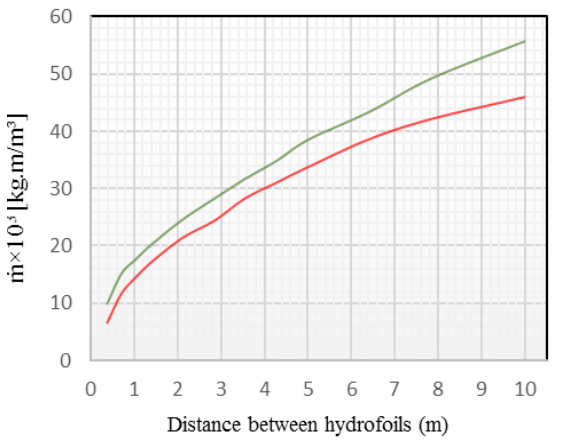

Figure 10. Mass flow rate ▫ behaviour according to the incense distance between the hydrofoils profiles.

Table 6. Mass flow ratio ε_m.

d (m)	ε_m
0.33	2.72
0.69	4.25
1.04	4.97
1.40	5.69
2.11	6.89
2.83	7.94
3.54	8.89
4.26	9.76
4.97	10.82
6.40	12.20
7.83	13.84
9.97	15.66

6. CONCLUSION

The present numerical study shows promising results regarding the applicability of the devices that use the Coanda effect. Results show that the numerical model employed here was successfully employed for representation of the main operational principle of the devices that use the Coanda effect. Moreover, it was possible to reach a theoretical recommendation about the influence of the distance between the hydrodynamic profiles over the mass flow rate in the device. For instance, amplification values for the mass flow rate reaching up to 1500% of efficiency.

With the results obtained in this study, a device with the configuration proposed by the authors would have practical applications in increasing the efficiency in flow machines such as pumps, compressors and blowers. The authors also recommend, as proposal for future studies, the creation of physical models for comparison with numerical results. In addition, the possibility of the use of 3D manufacturing can be applied to facilitate the construction of laboratory models, although studies of the mechanical proprieties and applications of polymer surfaces are still an open discussion in the literature [24].

In spite of the relative success in obtaining the effect of amplification of flow reached in this study, the numerical model must be improved to relax some simplifications employed in the present study. The evaluation of other turbulence modelling as well as the evaluation of forces in the device are a work in progress.

ACKNOWLEDGMENT

The author R. L. Lemos thanks Universidade Federal do Rio Grande for the support. M. dos S. Pereira thanks CAPES for financial support. L. A. O. Rocha, L. A. Isoldi and E. D. dos Santos thank CNPq for research grant.

REFERENCES

[1] H. Coanda, *Device for deflecting a stream of elastic fluid projected into an elastic fluid*. US2, 052,869, 1936.

[2] Mirkov, N., Rašuo, B., *Numerical Simulation of Air Jet Attachment to Convex Walls and Applications*, 27th ICAS Congress, 19 - 24 September, Nice, France, Pages: 1–7 (CD-Rom), 2010.

[3] Mirkov, N., Rašuo, B., *Maneuverability of an UAV With Coanda Effect Based Lift Production*, 28th ICAS CONGRESS, 23 - 28 September, Brisbane, Australia, Pages: 1–6 (CD-Rom). 2012.

[4] Mirkov, N., Rašuo, B., *Numerical simulation of air jet attachment to convex walls and application to UAV, In: Boundary and Interior Layers, Computational and Asymptotic Methods - BAIL 2014*, Editor: Knobloch, Petr, Series: Lecture Notes in Computational Science and Engineering, Vol. 108, Springer, pp. 197-208, ISBN 978-3-319-25727-9, 2015.

[5] Drãgan, V., *A New Mathematical Model for High Thickness Coanda Effect Wall Jets. Review of the Air Force Academy*. No. 1 (23), 2013.

[6] Dãgan, V., *A parametric study of a thick, incompressible flow over a curved surface*. Incas Bulletin, Vol. 3, No. 4, pp. 145-152, 2011.

[7] Cîrciu, I. and Boscoianu, M., *An analysis of the effieciency of Coanda – MOTAR anti-torque systems for small helicopters*. Anniversary Session Centennial celebration of the first jet aircraft invented by Henri Coanda organized by INCAS. Bucharest, Romania. 2010.

[8] Olivitto, C., *Fluidic Elements Based on Coanda Effect*. Incas Bulletin, Vol. 2, No. 4, pp. 163, 2010.

[9] Guoqi, L., et al., *Influence of Coanda Surface Curvature on Performance of Bladeless Fan*, Journal of Thermal Science, Vol. 23, No. 5, pp. 422 – 431, 2014.

[10] Afshin, H. et al., *Numerical Aerodynamic Evalu–ation and Noise Investigation of a Bladeless Fan*, Journal of Applied Fluid Mechanics, Vol. 8, No. 1, pp. 133 - 142, 2015.

[11] Valentín, D., Guardo, A., Egusquiza, E., Valero, C. and Alavedra, P., *Use of Coandă nozzles for double glazed façades forced ventilation*, Energy and Buildings, Vol. 62, pp. 605 – 614, 2013.

[12] Kumagai, I., Yoshiaki, T. Murai, Y., *Power-saving device for air bubble generation using a hydrofoil to reduce ship drag: Theory, experiments and application to ships.* Ocean Engineering Journal, Vol. 95, pp. 183-194, 2015.

[13] Fragassa C., *From Design to Production: an integrated advanced methodology to speed up the industrialization of wooden boats*. Journal of Ship Production and Design. Vol. 33, No. 2, pp. 1–10, 2017. Doi: 10.5957/JSPD.33.2.160022.

[14] Minak, G. et al.: *A brief review on determinant aspects in energy efficient solar car design and manufacturing. Sustainable Design and Manufacturing 2017*, Smart Innovation, Systems and Technologies series. Editors: Campana, G., Howlett, R. J., Setchi, R., Cimatti, B., Springer International Publishing AG2017, Chapt. 78, pp: 1-9, DOI: 10.1007/978-3-319-57078-5_76

[15] Betancur E. et al., Aerodynamic effects of manufacturing tolerances on a solar car. Sustainable Design and Manufacturing 2017, Smart Innovation, Systems and Technologies series. Editors: Campana, G., Howlett, R. J., Setchi, R., Cimatti, B., Springer International Publishing AG, 2017. Chapt. 78, pp. 1-9, DOI: 10.1007/978-3-319-57078-5_78

[16] Nikitakos, N., *The concept of Zero Emission Port.* FME Transactions, Vo 40, pp. 201-206, 2012.

[17] Wilcox, D. C., *Turbulence Modelling for CFD*, DCW Industries, La Canada, USA. 2002.

[18] Launder, B. E. and Spalding, D.B., *Mathematical Models of Turbulence*. Academic Press, London. 1972.

[19] Hinze, J. O, *Turbulence*, McGraw-Hill, New York, USA. 1975.

[20] Dos Santos, E. D., Rodrigues, M. P., Andrade, T. S. V. C., Isoldi, L. A., Franca, F. H. R. and Rocha, L. A. O., *Numerical Study of Different Closure Approaches for Prediction of Forced Convective Turbulent Cylindrical Cavity Flows*, Defect and Diffusion Forum, Vol. 366, pp. 166-181, 2016.

[21] Ansys Fluent, *Documentation Manual* – FLUENT 6.3.16. 2007.

[22] Cornell,University.<https://confluence.cornell.edu/display/SIMULATION/FLUENT+-Flow+over+an+Airfoil>. Acess: march 24, 2016.

[23] Abbott, I. H., Von Doenhoff A. E., *Theory of Wing Sections*. Dover Publications, NY. EUA. 1959.

[24] Pavlovic, A., Sljivic, M., Kraisnik, M., Ilic, J., Anic, J., *Polymers in additive manufacturimg the case of water pump impeller.* FEM Transactions, Vol. 45, No. 3, pp. 354-359, 2017.

NOMENCLATURE

A'	area unit as a function of the domain depth unit, m²/m
C_D	drag coefficient
C_L	lift coefficient
$C_{1\varepsilon}$, $C_{2\varepsilon}$, C_μ	Parameters of the standard model k-ε
k	kinetic energy of turbulence, kg/m^2
l	rope length of a profile, m
$\dot{m}_e$	mass flow in the road of the control volume, kg/s
$\dot{m}_s$	mass flow in the control volume output, kg/s
$\dot{m}_b$	mass flow in the nozzles, kg/s
p	static pressure, Pa
Re	Reynold's number
t	time, s
v	modulation of rotor frequency due to rotor damage, Hz
$\vec{V}$	velocity of a fluid in relation to the control surface, m/s
x,y,z	Cartesian coordinates

Greek symbols

σ_K, σ_ε	parameters of the standard model k-ε
ε	kinetic energy dissipation rate of turbulence, kg/m^2
ε_m	mass amplification ratio
τ_{ij}	shear stress tensor, N/m^2
τ_w	shear force acting on infinitesimal area, N
ρ	specific mass, kg/m^3
μ	dynamic viscosity, kg/m·s
μ_t	turbulent dynamic viscosity, kg/m·s
υ_t	turbulent kinematic visocisity, m^2/s

НУМЕРИЧКА АНАЛИЗА ТУРБУЛЕНТНОГ СТРУЈАЊА СА COANDA ЕФЕКТОМ КОД ХИДРОДИНАМИЧКИХ ПРОФИЛА

Р. Лемос, Р. Вијеира, Л. Изолди, Л. Роча, М. Переира, Е. Сантос

У поморској индустрији, хидро крилца се користе за производњу узгона код трупова са ниским трењем,

смањујући вучну силу између околног флуида и трупа. Ови уређаји се такође примењују да би одржали стабилност и управљивост брзих пловила. Недавна технологија заснована на Coanda ефекту за струјања преко хидродинамичких профила је развијена за примену ове опреме за повећање протока, претварањем силе узгона у погон, са циљем да фокусира интересовање индустрије за стварање побољшаних морских механизама потиска. Основна сврха овог рада је да симулира главни оперативни принцип хидро погонског уређаја на основу Coanda ефеката. Тачније, то се сматра турбулентним струјањем воде у два хидродинамичка профила. Проток воде у уређају је детаљно проучен у овом раду, решавањем нумерички средњег времена очувања једначине масе и момента коришћењем Computational Fluid Dynamics (CFD) кода на основу методе коначних запремина (FVM). За затворено моделирање турбуленције коришћен је стандардни k - ε модел.

Ефекат удаљености протока између два хидро–динамичка профила је такође студиран. Добијени резултати су показали да је умножавајући ефекат приметан у протоку воде у области између два хидродинамичка профила, што је слично претходним проналасцима из литературе за проток ваздуха кроз аеродинамичне профиле под утицајем Coanda ефекта.